

## TURBULENT FLAME STRUCTURE AND SPEED IN SPARK-IGNITION ENGINES

JAMES C. KECK

*Massachusetts Institute of Technology  
Cambridge, MA 02139*

Recent experimental observations of flame structure and speed in spark-ignition engines are discussed. Schlieren photographs, shadowgraphs and laser scattering measurements strongly suggest a highly wrinkled structure for the turbulent flame in such engines. Simultaneous pressure measurements and high-speed motion picture records are used to derive two closely related sets of empirical equations for calculating burning rates. One set suggests an eddy entrainment and laminar burn-out model and the other, a laminar flame stretching and wrinkling model. Tentative correlations relating the parameters in the burning equations to engine geometry and operating variables are derived. Statistical variations in the parameters produce cycle-to-cycle dispersions in the pressure, but correlations for predicting the magnitude of the dispersions have not yet been obtained.

### 1. Introduction

Spark ignition engines consume more than a billion gallons of gasoline daily or roughly one-third the total world petroleum production. They are also a major source of air pollution in urban areas. Thus increasing the fuel efficiency and reducing the pollution from these engines is a matter of considerable practical importance which has become a major goal of current combustion research. Of particular concern is the development of quantitative models for predicting the burning rate of the charge in spark-ignition engines.<sup>[1]</sup> Such models are needed both for interpreting the performance of existing engines and for improving the design of future engines.

As a result of studies carried out over more than half a century, it has been well established that the burning rate in spark-ignition engines involves a turbulent combustion process having significant cycle-to-cycle fluctuations. Although a great deal of experimental data has been accumulated and numerous theories have been proposed, a completely satisfactory model for predicting turbulent burning rates in spark-ignition engines has not yet been developed. A critical review of current theories of turbulence and their compatibility with different models of turbulent flame propagation has been made by Andrews, Bradley and Lwakabamba<sup>[2]</sup> and the application of such models to spark-ignition engines has been reviewed by Tabaczynski.<sup>[3]</sup>

It is clear from these reviews, as well as more recent publications,<sup>[4-9]</sup> that the development of models for turbulent combustion in spark-ignition engines based on fundamental principles is a for-

midable task unlikely to be completed in the near future. A simpler and more promising short range approach is the development of empirical models based on detailed correlations of experimental data and as free as possible from initial physical assumptions. An advantage of such models is that they can be used both for immediate practical applications in engine design and analysis and to obtain physical insight useful for developing and testing more fundamental models of turbulent combustion for future use.

The purpose of this paper is to discuss recent experimental observations of flame structure and speed in spark-ignition engines and to present two empirical burning models derived from them. The emphasis is on studies<sup>[10-17]</sup> in which simultaneous optical and pressure measurements have been made. The first measurements of this type were reported by Rassweiler and Withrow<sup>[18]</sup> who showed that flame geometry and pressure were strongly correlated. Unfortunately, these authors did not include sufficient data to permit quantitative correlation of their results with engine geometry and operating variables. This is also true of a number of other investigations<sup>[19-30]</sup> from which only qualitative conclusions can be drawn. In all cases, however, the qualitative conclusions support the quantitative results discussed in this paper.

Because the primary objective of this paper is to examine the manner in which burning rates in spark-ignition engines are correlated with engine geometry and operating variables, no discussion of turbulence measurements in engines, theories of turbulent combustion, or burning models based on a priori assumptions is included. Reviews of these

TABLE 1  
S.I. Engine parameters

Author	$b$ mm	S mm	CR	$h_{TC}$ mm	$L_{IV}$ mm	$D_{IV}$ mm	Ref.
Mattavi, et al.	92.1	76.2	6.9	13.0	5.6	41.8	12, 13
Rashidi, M.	101.6	88.9	7.9	13.0	9.3	48.3	14
Namazian et al.	82.6	114.3	4.8	30.1	5.7	31.5	16
Witze; Smith	76.5	82.6	5.5	18.3	4.8	12.7	16, 17
Blizard & Keck	63.5	76.2	5.0	19.0	4.8	24.9	18
Lancaster, et al.	92.1	76.2	6.9	13.0	5.6	41.8	11

$b$  = bore, S = stroke, CR = compression ratio,  $h_{TC}$  = Top center clearance height,  $D_{IV}$  = inlet valve diameter,  $L_{IV}$  maximum inlet valve lift.

important topics may be found in Refs. 2, 3, 5 and 9.

## 2. Experimental Observations

All of the experiments discussed in this paper were carried out in single cylinder research engines equipped with windows providing optical access.<sup>[12-17]</sup> Their important geometrical specifications are summarized in Table 1. Also included are the specifications for the engines used by Blizard and Keck<sup>[10]</sup> and Lancaster, Krieger, Sorenson and Hull<sup>[11]</sup> in earlier investigations the results of which are included in Section 4.

### 2.1 Visible Emission Photography

One of the most extensive studies of the relationship between flame geometry and pressure is that carried out by Rashidi<sup>[14]</sup> in an engine equipped with a quartz piston. Similar studies have also been carried out by Mattavi, Groff, Lienesch, Matekunas and Noyes<sup>[12]</sup> and Groff and Matekunas.<sup>[13]</sup>

A schematic of the engine used by Rashidi which was based on a design due to Bowditch<sup>[31]</sup> is shown in Fig. 1. To enhance the luminosity of the hot burned gases, the charge was seeded with NaCl in a heated mixing tank. High-speed motion pictures of the expanding flame were made using a rotating-prism camera and synchronized pressure records were made using a silicone-coated piezoelectric transducer coupled to an analog-to-digital recorder.

To avoid overheating the quartz window, the engine was fired in short bursts of 10 to 15 consecutive cycles. A typical set of pressure traces from such a burst is shown in Fig. 2. The "motored cycle" was obtained just prior to switching on the ignition and provided both a useful reference curve and a check on the absolute calibration of the pressure transducer. Due to the absence of residual burned gases in the charge, the first cycle has a

higher peak pressure and a shorter burning time than later cycles. The residual fraction for all cycles following the first was  $f_r = 0.2$  and was determined from the thermodynamic analysis of the pressure traces discussed in Section 3.1. Although later cycles show substantial cycle-to-cycle fluctuations in pres-

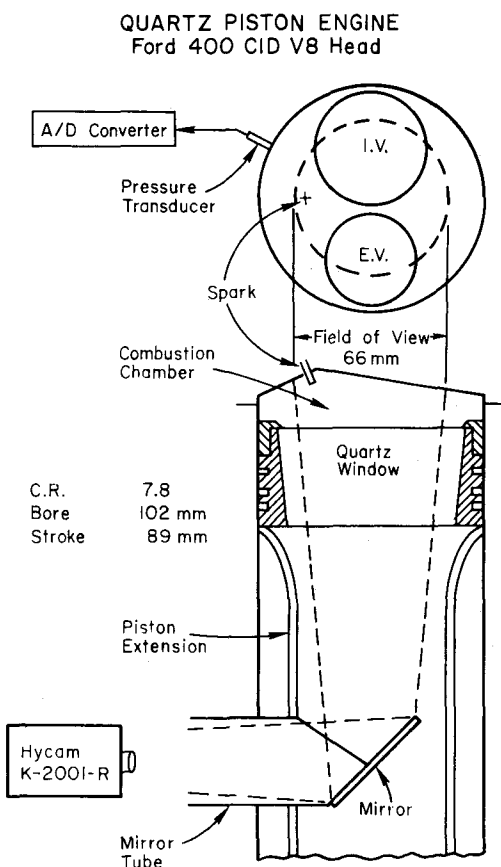


FIG. 1. Schematic of the M.I.T. quartz piston spark-ignition engine used by Rashidi.

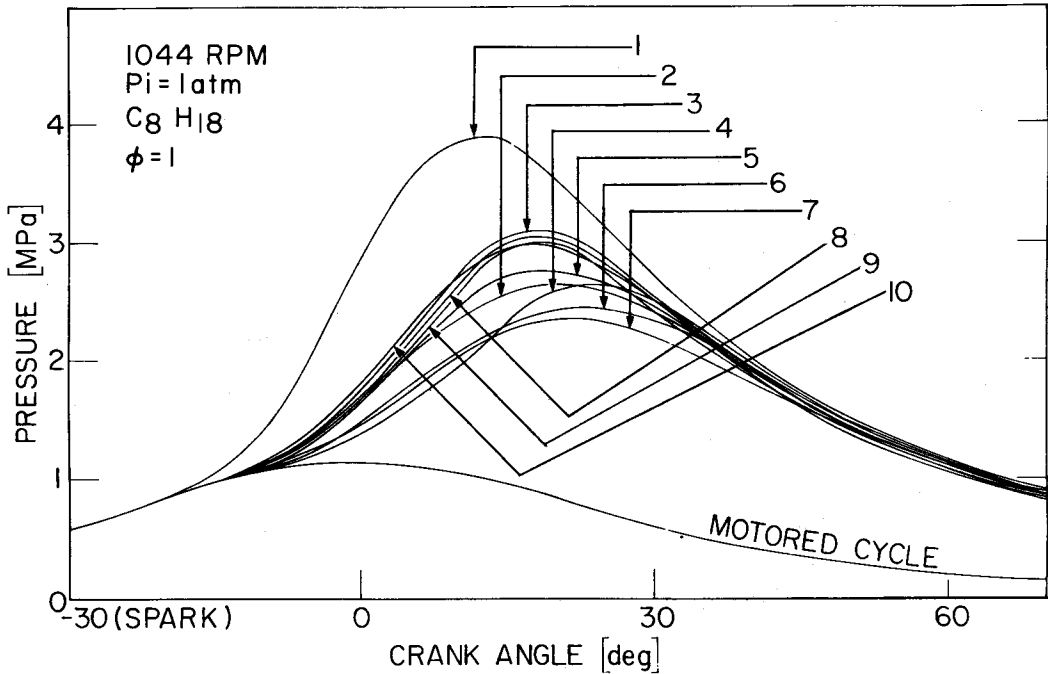


FIG. 2. Typical sequence of pressure vs crank angle traces from the M.I.T. quartz piston engine.

sure, there is no evidence that the second cycle differs significantly from those following it, indicating that relaxation to steady-state operation occurs in one cycle.

A typical photographic record of an expanding flame is shown in Fig. 3. The engine operating conditions for this cycle are given at the top of the figure and the pressure record is shown by curve 5 in Fig. 2. The crank angle  $\theta$  and the ratio  $p/p_m$  of the pressure to the motored pressure are given below each frame. The interval between frames is 1.9 crank angle degrees or roughly one-third of a millisecond. Note that spark occurred at a crank angle of  $-30^\circ$  ATC and that the first 5 frames during which the image was too weak to record satisfactorily have been omitted. It can be seen that the edge of the fireball is reasonably well defined and similar in appearance to the edge of a cloud. It can also be seen that during the first few frames in which the flame is clearly visible the increase in pressure above the motored pressure is very small. Thus optical observations provide a much better indication of the progress of the combustion at early times than pressure measurements.

2.2 Schlieren Photography

Although high-speed motion pictures of the visible emission from a flame provide a satisfactory method for locating the front, they give very little

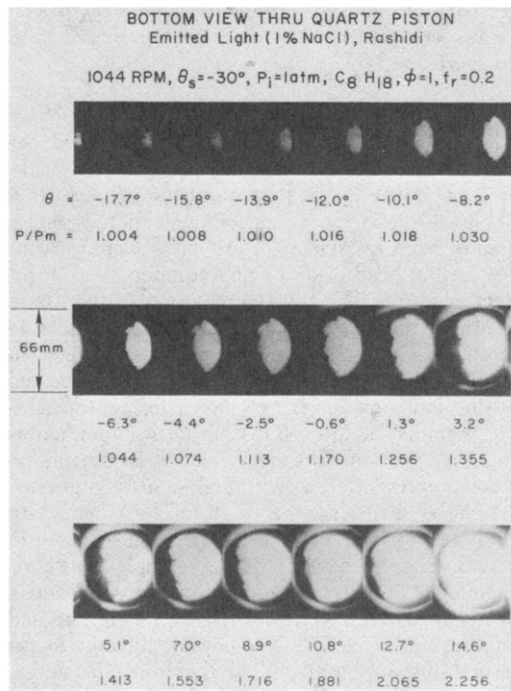


FIG. 3. Typical high-speed motion picture record of flame propagation in the M.I.T. quartz piston engine. (Cycle 5 of Fig. 2.)

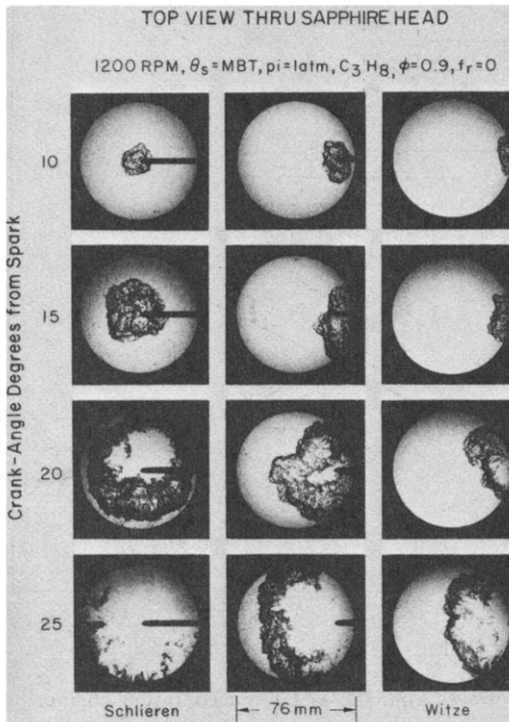


FIG. 4. Schlieren photographs showing the effect of spark location on turbulent flame structure at various crank angles in a spark-ignition engine with no swirl.

information about the structure of the flame behind the front. To obtain such information, schlieren photography has been used.

Fig. 4 shows a typical set of schlieren photographs taken by Witze<sup>[16]</sup> through a sapphire window in the head of an engine equipped with a reflecting piston. The engine operating conditions are shown at the top of the figure and are similar to those for Fig. 3. Each photograph was obtained on a different engine cycle at the crank angle indicated on the left. Sequences are shown for central ignition, ignition at three fifths of the cylinder radius and wall ignition. The dark regions of the photographs represent zones with high density gradients. It can be seen that the fronts of the flames are very well defined and similar in shape to those in Fig. 3. Because a schlieren photograph represents an integrated effect along the line of sight and a mirror image of the flame has been superimposed on the real image, it is somewhat difficult to interpret the structure behind the front. However, it appears that the unburned and burned gas in these photographs is separated by a wide zone having a mottled structure more suggestive of a highly wrinkled thin laminar flame than a thick turbulent

flame with a smoothly varying density gradient.

A more detailed picture of the structure of a turbulent flame is provided by the enlarged schlieren photographs shown in Fig. 5. These photographs were taken by Namazian et al.<sup>[15]</sup> using a square piston engine equipped with quartz windows through which the flame front could be viewed from the side. The top photograph was taken at a relatively early stage of the burning process and strongly suggests a thin, moderately wrinkled, but simply connected front between unburned and burned gas. The thickness of the front as shown by the width of the dark lines in the photograph is less than 0.1 mm. This is comparable to the thickness of the thermal preheat zone of a laminar flame under the prevailing conditions. The typical scale of the wrinkles is  $\sim 2.5$  mm. The structure of the flame at later times is shown in the two lower photographs. It can be seen that the width of the dark lines remains roughly constant but the

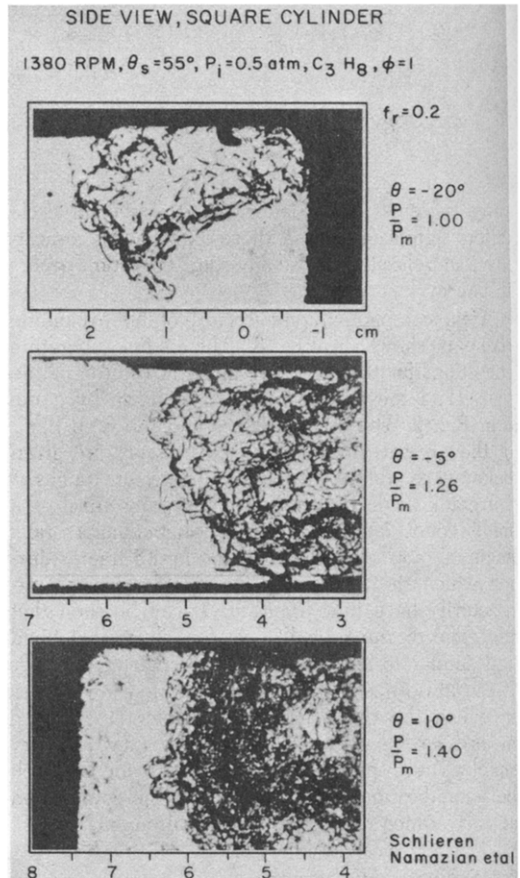


FIG. 5. Schlieren photographs showing side views of turbulent flames in a square piston spark-ignition engine at various crank angles.

scale of the wrinkles tends to decrease with time suggesting a decrease in the turbulent length scale due to compression of the unburned gas.

### 2.3 Laser Scattering

As already observed, the interpretation of schlieren photographs is complicated by the fact that they represent integrated effects along the line of sight. This difficulty has been overcome in the elegant laser scattering measurements made by Smith.<sup>[17]</sup> A schematic diagram of the engine cylinder and optical arrangement used for these measurements is shown in Fig. 6. A pulsed laser beam was passed across the cylinder and the Rayleigh scattered light from the gas molecules was recorded by an optical-multichannel-analyzer focused on the beam. The duration of the laser pulse was  $0.01 \mu\text{s}$ , the diameter of the beam was  $0.05 \text{ mm}$  and the spatial resolution along the axis of the beam was  $0.14 \text{ mm}$ . Using this system, Smith was able to obtain "snap shots" of the density profile along the axis of the laser beam.

A selected oscillogram of the output of the optical analyzer is shown in Fig. 7a. Each dot represents the intensity of the scattered light in one channel. The signal on the left corresponds to unburned gas and that on the right to burned gas. The oscillogram shows a thin transition zone of width  $0.25 \text{ mm}$  between unburned and burned gas followed at a distance of  $1.5 \text{ mm}$  by an "island" of

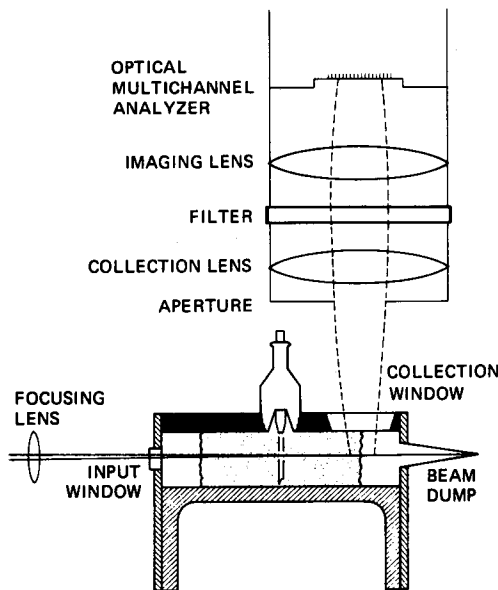


FIG. 6. Schematic diagram showing engine cylinder and optical train used in Smith's laser scattering experiments.

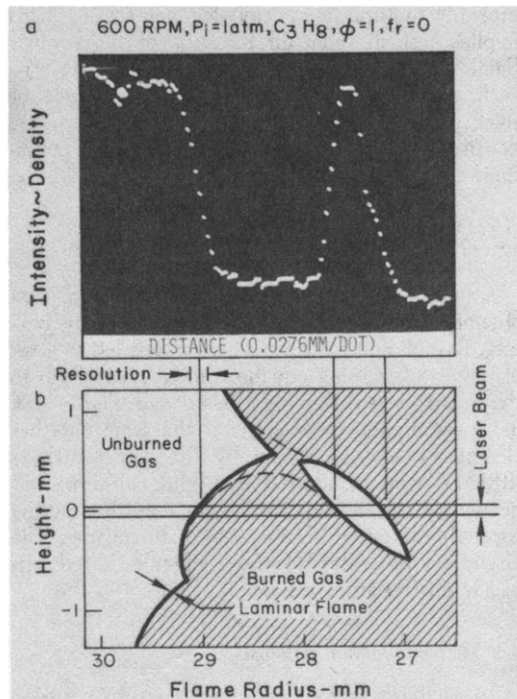


FIG. 7(a). Selected oscillogram of the output of Smith's optical-multichannel-analyzer showing the scattered intensity in various channels. (b) "Author's Conception" of a possible flame geometry associated with the observed scattering pattern.

unburned gas. The fraction of oscillograms showing such "islands" varied from 0 at 300 RPM to 20% at 1800 RPM. The present "author's conception" of the flame front geometry associated with a signal of this type is shown in Fig. 7b. The thickness of the laminar flame shown was calculated by Westbrook.<sup>[17]</sup>

Note that the widths of the observed transition zones are not significantly greater than those expected from a convolution of a tilted laminar flame and the resolution function. In this connection it should be noted that the most probable tilt angle of a highly wrinkled flame front is not zero, as Smith assumed, due to the fact that the solid angle available for the local normal vector to the flame front vanishes at zero tilt angle. In Fig. 7b, the unburned gas behind the leading front is shown as an "island" which is the interpretation favored by Smith. It could, of course, also be a "peninsula" as shown by the dashed curve.

In the opinion of the author, Smith's laser scattering experiments coupled with the schlieren photographs discussed earlier provide convincing evidence that fully developed turbulent flames in spark ignition engines are indeed highly wrinkled and

probably multiply connected laminar flames. This implies a small value for the ratio of the laminar flame thickness to the turbulence length scale in such engines. No evidence for the existence of thick turbulent flames with monotonically varying density profiles has been found under any conditions studied to date.

### 3. Correlation of Pressure and Flame Geometry

A preliminary analysis of the experimental data obtained by Rashidi<sup>[14]</sup> has been reported by Beretta, Rashidi and Keck.<sup>[32]</sup> This analysis led to a set of empirical burning equations identical in form to those proposed earlier by Blizard and Keck.<sup>[10]</sup> A more comprehensive analysis of the same data has recently been completed by the same authors (BRK)<sup>[33]</sup> who found that an additional term was needed in the Blizard-Keck equations to describe correctly the initial burning rate of the charge. The discussion presented in this section is based primarily on the latter report.

#### 3.1 Thermodynamic Analysis

To establish a quantitative relationship between pressure and flame geometry in spark ignition engines, it is necessary to have an accurate thermodynamic model for obtaining the mass fraction of burned gas from the observed cylinder pressure. The model used by BRK is a refinement of the model originally developed by Lavoie et al.<sup>[34]</sup> and includes the important effects of gas cycled in and out of crevices as well as the usual heat and mass loss corrections. The basic assumptions of the model are (i) the charge in the combustion chamber at any time can be divided into a mass fraction burned separated from a mass fraction unburned by a reaction zone of negligible volume; (ii) the pressure is spatially uniform; (iii) both unburned and burned gases have slowly varying specific heats and obey the ideal gas equation of state; (iv) the composition of the unburned gas is frozen while that of the burned gas is in chemical equilibrium; (v) the gas in the crevices is at the wall temperature and (vi) the unburned gas in the control volume is isentropically compressed. Note that assumption (i) which has been included in virtually all thermodynamic models of combustion in closed chambers has now been justified by the optical observation discussed in Section 2.

As a result of these assumptions the equations for volume and mass become

$$V_c = V_u + V_b \quad (3.1)$$

and

$$m_c = m_u + m_b \quad (3.2)$$

where the subscripts *v*, *u* and *b* denote the combustion chamber volume, the unburned gas and the burned gas respectively. The mass and volume fractions burned are defined by

$$x_b = m_b/m_c \quad (3.3)$$

and

$$y_b = V_b/V_c \quad (3.4)$$

and the mean burned and unburned gas densities by

$$\rho_b = m_b/V_b = p/R_b T_b \quad (3.5)$$

and

$$\rho_u = m_u/V_u = p/R_u T_u \quad (3.6)$$

Using these equations and submodels for heat and mass transfer, the energy equation for the combustion chamber can then be solved to obtain the mass fraction burned as a function of the pressure.

Fig. 8 shows the results of such a thermodynamic analysis applied to the pressure curves for the first 5 cycles of Fig. 2. Part (a) shows the mass fraction burned  $x_b$  as a function of crank angle

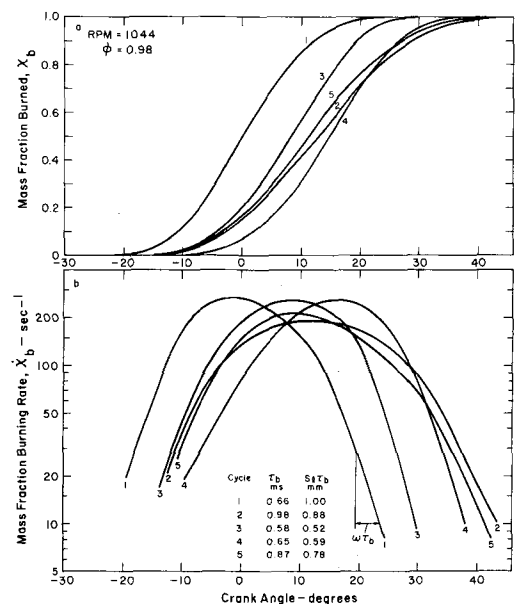


FIG. 8. (a) Typical mass fraction burned curves calculated from the pressure records for cycles 1-5 of Fig. 2. (b) Mass fraction burning rate curves obtained by taking the time derivative of the curves in (a).

while the lower part shows the corresponding burning rate  $\dot{x}_b$ .

As previously noted, the charge for the first cycle contains no unburned residual gas and this is the cause of the significantly smaller "ignition delay" for this cycle. Later cycles show substantial cycle-to-cycle fluctuations in both the magnitude and shape of the burning rate curves but again there is no evidence that the second cycle differs significantly from those following it. The final burning rates can be approximated by exponential decays having characteristic time constants  $\tau_b$  varying from 0.6 to 1.0 ms as given in the figure. Also given are the corresponding characteristic lengths

$$\ell_T = s_\ell \tau_b \quad (3.7)$$

obtained by multiplying  $\tau_b$  by the laminar burning speed  $s_\ell$ . Geometrical data to be discussed later show that the exponential burning phase occurs after all the charge in the control volume has been fully entrained in the flame. This is consistent with the existence of "islands" of unburned gas behind the leading edge of the flame.

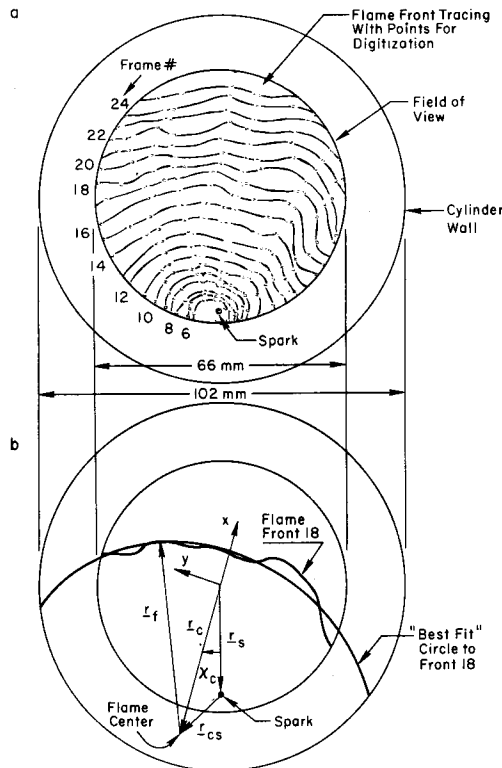


FIG. 9. (a) Superimposed tracings of the successive flame fronts shown in Fig. 3. (b) Illustration showing "best fit" circle to flame front 18.

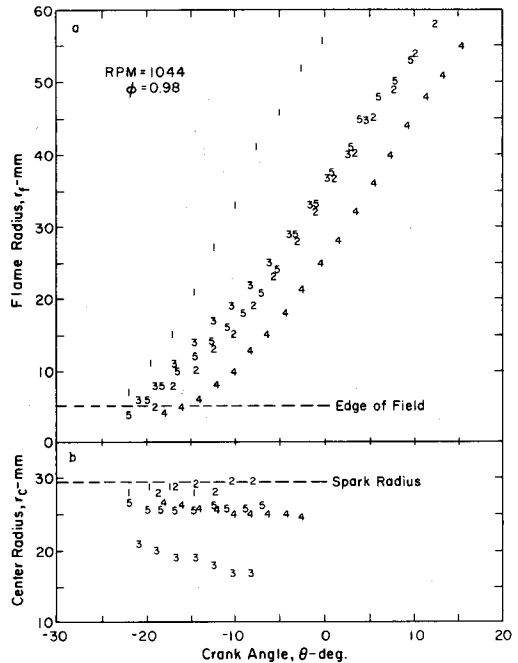


FIG. 10. (a) Typical plot of "best fit" flame radius  $r_f$  as a function of crank angle  $\theta$  for cycles 1-5 of Fig. 2. The points (cycle numbers) correspond to individual frames of the motion picture record. The "edge-of-field" line shows the radius beyond which only part of the flame front is visible. (b) Plot of corresponding flame center radius  $r_c$ .

### 3.2 Flame Geometry

Using motion picture records of the type shown in Fig. 3, Rashidi has made contour plots of the leading edge of the flame in successive frames for more than 100 cycles covering a range of operating conditions. A plot of this type made from the photographs in Fig. 3 is shown in Fig. 9a. It can be seen that due to the limited field of view a substantial part of the flame front was not observable.

To reconstruct the flame front and to obtain the effective fireball volume, BRK have used the method of least squares to obtain "best fit" circles to the observable portion of the flame fronts. In making the fit the radius of the circle and the position of the center are the parameters to be determined and the "best fit" circle is required to enclose the same area as the observed flame front. The coordinate system employed and an example of such a fit are shown in Fig. 9b.

Fig. 10 shows the "best fit" flame radius  $r_f$  and center radius  $r_c$  as a function of crank angle for the first 5 cycles of Fig. 2. For flame radii less than 4 mm, the images were too weak for the edge to be clearly defined, while for flame radii greater

than 20 mm, the angle subtended by the observed front was too small to permit accurate determination of the center radius.

It can be seen that the expansion speed of the flame increases with radius, approaching a very nearly constant value for radii greater than approximately 20 mm. It can also be seen that there is a significant radial displacement of the flame center from the spark most of which occurs before the flame has grown sufficiently in radius to become clearly visible. This can be attributed to convection of the flame kernel by a "squish" flow which for cycle 3 has a mean speed of  $\sim 6$  m/s.

To obtain the enflamed volume  $V_f$  and frontal area  $A_f$ , it is necessary to consider the third dimension and BRK have assumed that  $A_f$  may be approximated by a spherical surface of radius  $r_f$  with its center located at the same radial and angular position as the "best fit" circle and at the same height as the spark.

3.3 Correlation of Thermodynamic and Geometrical Data

To facilitate the comparison of the thermodynamic and geometrical data, BRK have introduced the following basic definitions:

(i) the burned gas radius  $r_b$  defined by the equation

$$V_b(r_b, r_c, h) \equiv V_b(p, \theta), \tag{3.8}$$

where  $h = V_v/A_p$  is the mean combustion chamber height,  $A_p$  is the piston area,  $r_c$  is the position of the flame center and  $r_b$  is the radius of the spherical surface concentric with the flame front which contains the burned gas mass;

(ii) the spherical burning area

$$A_b \equiv \partial V_b(r_b, r_c, h) / \partial r_b; \tag{3.9}$$

(iii) the laminar burning area

$$A_\ell \equiv (dm_b/dt) / \rho_u s_\ell, \tag{3.10}$$

where  $s_\ell$  is the laminar burning speed;

(iv) the mean expansion speed of the flame front

$$u_f \equiv (dA_c(r_f, r_c, \chi_c) / dt) / L_c, \tag{3.11}$$

where  $A_c(r_f, r_c, \chi_c)$  is the "shadow" area enclosed by the "best fit" circle through the leading edge of the flame front and

$$L_c = \partial A_c(r_f, r_c, \chi_c) / \partial r_f \tag{3.12}$$

is the arc length of the "best fit" circle;

(v) the mean expansion speed of the burned gas

$$u_b \equiv (\partial V_b / (r_b, r_c, h) / \partial t) / A_b; \tag{3.13}$$

(vi) the burning speed

$$s_b = (dm_b/dt) / \rho_u A_b; \tag{3.14}$$

(vii) the mean gas speed

$$u_g = u_b - s_b. \tag{3.15}$$

It follows from Eqs. 3.10 and 3.14 that

$$s_b A_b = s_\ell A_\ell \tag{3.16}$$

It also follows from Eqs. 3.1, 3.2, 3.4, 3.5, 3.6, 3.13 and 3.14 that

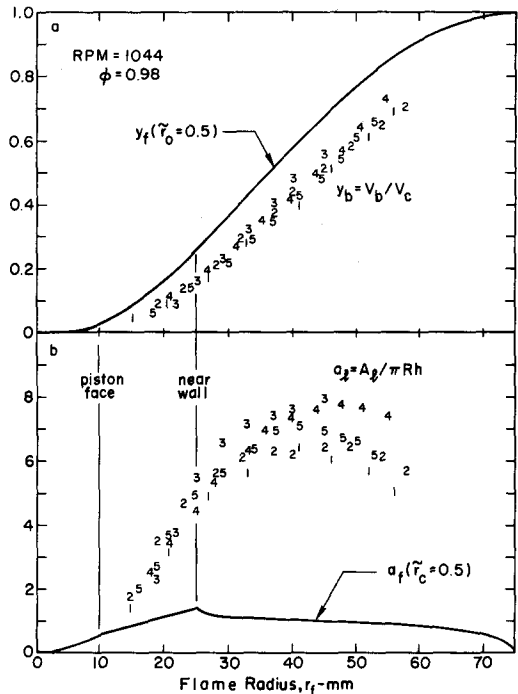


FIG. 11. (a) Comparison of burned gas volume fraction  $y_b$  for cycles 1-5 of Fig. 2 and enflamed volume fraction  $y_f$  as a function of flame radius  $r_f$ . A mean value of 0.5 was assumed for  $\bar{r}_c = r_c/R$  in calculating  $y_f$ . (b) Comparison of the dimensionless laminar burning area  $a_\ell$  and the dimensionless flame area  $a_f$ . Note that discontinuities in the derivative of  $a_f$  occur when the flame front impinges on the piston face and the near wall.

$$u_b \equiv \left( \frac{m_v}{\rho_b V_v} \right) s_b = \left( \frac{\rho_u}{\rho_b} (1 - y_b) + y_b \right) s_b, \quad (3.17)$$

where the piston speed has been assumed small compared to the expansion speed  $u_b$ . Note that for  $y_b = 0$ ,  $m_v/V_v = \rho_u$  and  $m_v/\rho_b V_v = \rho_u/\rho_b$  is just the expansion ratio.

A comparison of the burned gas volume fraction  $y_b$  and the enflamed volume fraction  $y_f$  as a function of the flame radius  $r_f$  is shown in Fig. 11a for the first 5 cycles of Fig. 2 and a comparison of the corresponding dimensionless laminar burning area  $a_\ell = A_\ell/\pi R h$  with the dimensionless flame area  $a_f = A_f/\pi R h$  is shown in Fig. 11b. Discontinuities in the derivative of  $a_f$  occur at the points where the flame front first touches the piston face and the near wall. It can be seen in Fig. 11a that during the rapid burning region from  $y_f \sim 0.2$  to  $0.7$  a significant fraction of the gas entrained in the fireball is unburned. It can also be seen in Fig. 11b that during this phase the laminar burning area exceeds the flame front area by almost a factor of 10. Both these observations are consistent with the existence of a wrinkled laminar flame suggested by the optical observations discussed in Section 2.

An interesting comparison suggested by the data in Fig. 11 is shown in Fig. 12a where the differences  $(V_f - V_b)$  and  $(A_\ell - A_f)$  have been plotted on a logarithmic scale as a function of  $r_f$ . It can be seen that the two sets of points are remarkably similar in shape suggesting that their ratio should be approximately constant. This ratio

$$\ell_T = (V_f - V_b)/(A_\ell - A_f) \quad (3.18)$$

which has been identified with the characteristic length defined by Eq. 3.7 is of the order of 1 mm and is shown in Fig. 12b. Although there is considerable cycle-to-cycle scatter, the points for any one cycle are quite consistent and suggest a slight decrease in  $\ell_T$  with increasing  $r_f$ .

The expansion speeds  $u_f$  calculated from Eq. 3.11 are shown as a function of flame radius  $r_f$  by the upper set of points in Fig. 13a. Also shown are the corresponding burning speeds  $s_b$  obtained from Eq. 3.17 and the laminar burning speeds  $s_\ell$  for isoctane measured by Metghalchi and Keck.<sup>[35]</sup> The difference between  $u_b$  and  $s_b$  is, of course, the gas speed  $u_g$  at the front.

It can be seen that  $s_b$  accelerates from a value very close to  $s_\ell$  to a value of order 10 times  $s_\ell$  as  $r_f$  increases from 0 to 50 mm. It can also be seen that the value of the difference  $(s_b - s_\ell)$  for the first cycle does not differ significantly from that for later cycles suggesting that  $(s_b - s_\ell)$  is independent of chemistry.

Fig. 13b shows the ratio  $s_b/s_\ell$  as a function of  $r_f$ . By definition this ratio is also equal to the ratio

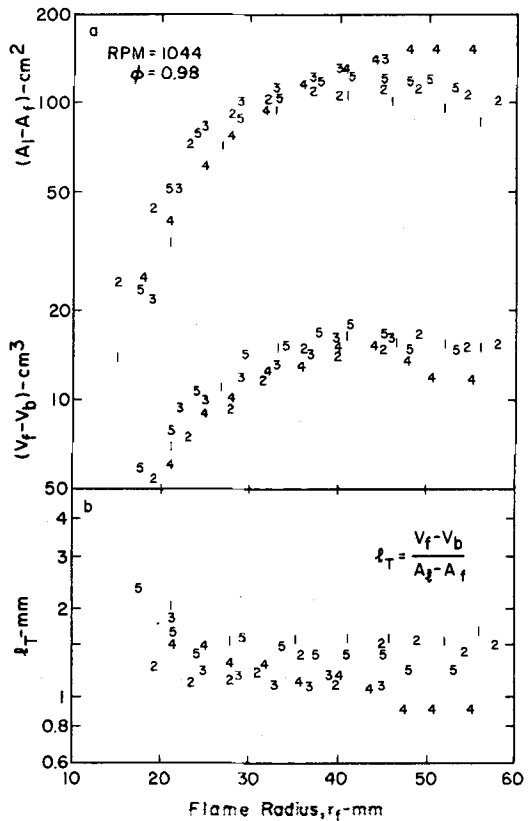


FIG. 12. (a) Plots of  $(A_\ell - A_f)$  and  $(V_f - V_b)$  for cycles 1-5 of Fig. 2 as a function of  $r_f$ . (b) The corresponding characteristic length  $\ell_T = (V_f - V_b)/(A_\ell - A_f)$ .

$A_\ell/A_b$  of the laminar burning area to the spherical burning area. This suggests that the increase in  $s_b$  is simply the result of the increase in laminar burning area produced by wrinkling of the flame front as it expands. Note that the ratio  $s_b/s_\ell$  for large  $r_f$  is significantly lower for the first cycle than for the following cycles due to the higher laminar burning speed of the charge for the first cycle.

#### 4. Turbulent Burning Equations and Correlations

The experimental results discussed above have been used to derive two closely related sets of empirical burning equations for spark-ignition engines and to obtain correlations relating the parameters in these equations to engine geometry and operating variables. These equations and correlations are discussed in this section. Also included are some recent observations of hydrogen and propane combustion in a spark-ignition engine which show the dominant influence of the laminar flame speed

on the initial burning rate and provide a critical test of the empirical burning equations.

#### 4.1 Eddy Burning Equations

Based on their analysis of Rashidi's data, BRK have derived the following empirical burning equations:

$$\frac{dm_b}{dt} = \rho_u A_f s_\ell + \frac{\mu}{\tau_b} \quad (4.1A)$$

$$\frac{d\mu}{dt} = \rho_u A_f u_T - \frac{\mu}{\tau_b} \quad (4.1B)$$

where

$$\mu = \rho_u \ell_T (A_\ell - A_f), \quad (4.2)$$

is a parametric mass,  $u_T$  is a characteristic speed and  $\tau_b = \ell_T/s_\ell$ .

To complete this set of equations, a relation between  $r_f$  and  $r_b$  must be specified. The experimental data suggest that  $r_f/r_b \rightarrow 1$  as  $r_f \rightarrow 0$  and  $(r_f - r_b) \rightarrow u_T \tau_b$  as  $r_b \rightarrow \infty$ . An empirical equation which approximates the data and satisfies these limiting conditions is

$$r_f = r_b + u_T \tau_b (1 - \exp(-(r_b/u_T \tau_b)^2)) \quad (4.3)$$

Equations 4.1 are similar to those previously proposed by Blizard and Keck but contain the important additional term  $\rho_u A_f s_\ell$  in Eq. 4.1A. This term is necessary to describe correctly the dependence of the initial burning rate on the laminar flame speed  $s_\ell$ .

#### 4.2 Flame Stretching Equations

During the preparation of this review, the author developed an alternative equally valid set of empirical burning equations. These equations were inspired by the work of Alun Thomas<sup>[36]</sup> on the application of "flame stretching" theories to combustion in spark-ignition engines and can be written in the form:

$$\frac{dm_b}{dt} = \rho_u A_f s_\ell + \frac{\rho_u \ell_T \eta}{\tau_b} \quad (4.4A)$$

$$\rho_u \ell_T \frac{d\eta}{dt} = \rho_u A_f u_T - \frac{\rho_u \ell_T \eta}{\tau_b} \quad (4.4B)$$

where

$$\eta = A_\ell - A_f \quad (4.5)$$

is a parametric area.

In the case where  $\rho_u \ell_T$  is a constant,  $\rho_u \ell_T \eta = \mu$  and Eqs. 4.4 and 4.1 are mathematically identical. In practice  $\rho_u \ell_T$  is slowly varying and Eqs. 4.1 and 4.4 fit the available data equally well.

It should be emphasized that the names "eddy burning" and "flame stretching" assigned to Eqs. 4.1 and 4.4 were suggested by the form of the equations and are not associated with any a priori physical models. Whether physical models corresponding to these equations can in fact be found is an open question requiring further study.

#### 4.3 Limiting Cases

The behavior of Eqs. 4.1 and 4.4 in four important limits is given below:

$$(i) \text{ quiescent charge, } u_T \rightarrow 0 \text{ or } \ell_T \rightarrow \infty$$

$$s_b \cong s_\ell \quad (4.6)$$

$$(ii) \text{ quasi-steady state, } d\mu/dt \cong 0 \text{ or } d\eta/dt \cong 0,$$

$$s_b \cong u_T + s_\ell \quad (4.7)$$

$$(iii) \text{ initial burning, } t \leq \tau_T = \ell_T/u_T,$$

$$\frac{s_b}{s_\ell} = \frac{A_\ell}{A_b} \cong 1 + \frac{t}{3\tau_T} = 1 + \frac{\rho_b u_T r_f}{3\rho_u s_\ell \ell_T}; \quad (4.8)$$

$$(iv) \text{ final burning, } t \geq t_F (A_f = 0)$$

$$\frac{A_\ell}{A_{\ell F}} = \frac{\dot{m}_b}{\dot{m}_{bF}} \cong e^{-(t-t_F)/\tau_b} \quad (4.9)$$

These limiting expressions were suggested by the experimental data and were used in determining the form of both sets of empirical burning equations.

#### 4.4 Parameters for Burning Equations

Each set of burning equations contains three parameters  $s_\ell$ ,  $u_T$  and  $\ell_T$  which in principle could be obtained from fundamental chemical kinetic and turbulence models but which at present must be determined experimentally.

The laminar flame speed  $s_\ell$  can be measured using laboratory burners and constant volume bombs and values are already available for a variety of practical fuels burning under engine-like conditions.

The characteristic speed  $u_T$  can be obtained either from optical data of the type shown in Fig. 13 or from measurements of the mass burning rate using Eqs 3.14 and 4.7. Within experimental error  $u_T$  is proportional to  $\sqrt{\rho_u}$  and a summary of currently available measurements is given in Fig. 14 which

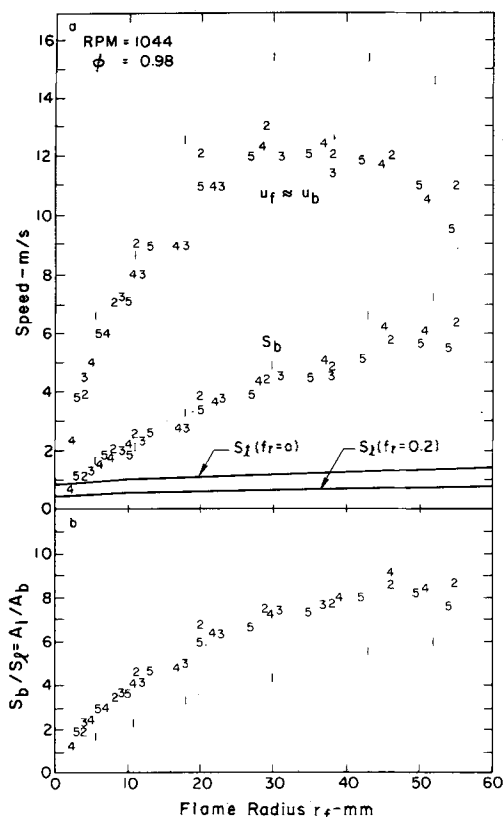


FIG. 13. (a) Plots of expansion speed  $u_f \approx u_b$  and the corresponding burning speed  $s_b$  for cycles 1-5 of Fig. 2 as a function of flame radius  $r_f$ . Also shown is the laminar burning speed  $s_\ell$  for 0 and 20 percent residual burned gas fractions. (b) Corresponding ratios  $s_b/s_\ell = A_\ell/A_b$ .

shows  $u_T \sqrt{\rho_i/\rho_u}$  as a function of the mean inlet gas speed  $\bar{u}_i = \epsilon_v(A_p/A_{IV})2NS$ , where  $\rho_i$  is the inlet gas density,  $\epsilon_v$  is the volumetric efficiency,  $A_p$  is the piston area,  $A_{IV}$  is the maximum open area of the inlet valve,  $N$  is the engine speed and  $S$  is the stroke. It can be seen that the measurements are correlated within  $\pm 10\%$  by the equation

$$u_T = 0.08 \bar{u}_i \sqrt{\rho_u/\rho_i} \quad (4.10)$$

Values of the characteristic length  $\ell_T$  obtained from available engine data are shown in Fig. 5 where the ratio of  $\ell_T$  to the maximum inlet valve lift  $L_{IV}$  is shown as a function of the ratio  $\rho_u/\rho_i$ . The points shown as circles were taken from BRK and show the variation of  $\ell_T$  during combustion. The remaining points were calculated by the author from data in the references cited using Eqs 4.1 and all refer to conditions at spark. Note that the values of  $\ell_T$  found from the data of Blizard and Keck dif-

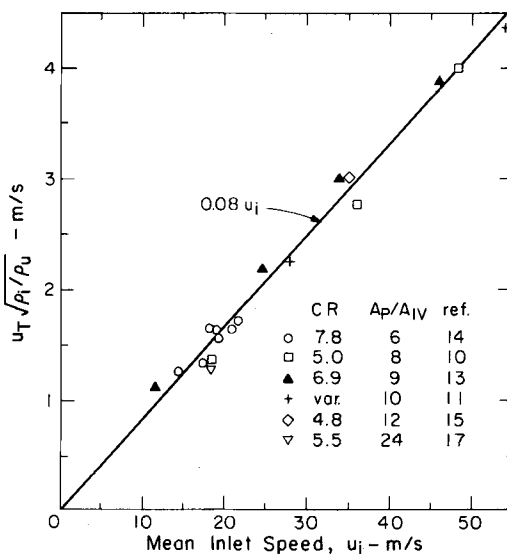


FIG. 14.  $u_T \sqrt{\rho_i/\rho_u}$  as a function of inlet gas speed  $u_i$ .

fer from those given in their paper due to the inclusion of the term  $\rho_u A_f s_\ell$  in Eq. 4.1A.

Although there is considerable scatter in the data,  $\ell_T$  appears to scale with valve lift  $L_{IV}$  rather than clearance height  $h_{TC}$  and to decrease with increasing density at a rate proportional to  $\rho_u^{-3/4}$ . Whether there is a dependence on inlet speed is not clear from the available data but, if there is, it is relatively weak. The results in Fig. 15 imply

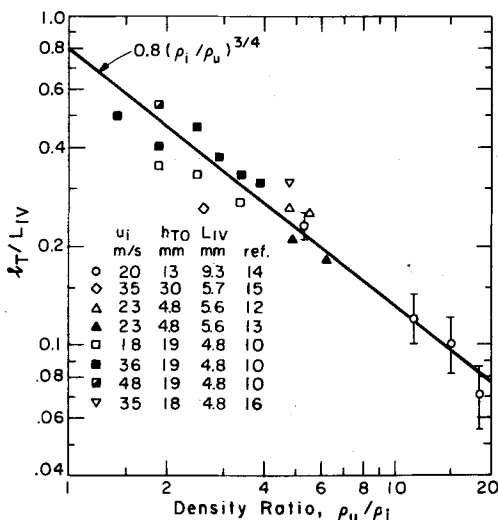


FIG. 15. The ratio of  $\ell_T$  to the inlet valve lift  $L_{IV}$  as a function of the ratio of the unburned gas density  $\rho_u$  to the inlet density  $\rho_i$ .

a correlation of the form

$$\ell_T = 0.8 L_{IV}(\rho_i/\rho_u)^{3/4} \quad (4.11)$$

with a standard deviation of about  $\pm 25\%$ .

4.5 Hydrogen-Propane Comparison

A critical test of the proposed turbulent burning equations 4.1 and 4.4 is provided by the schlieren photographs of combustion in hydrogen/air and propane/air mixtures shown in Fig. 16. These photographs were obtained in a recent investigation by Vilchis and Heywood<sup>[37]</sup> using M.I.T.'s square piston engine.<sup>[15]</sup> The difference in the combustion process shown for these two gases is dramatic. In hydrogen, the induction time has been virtually eliminated and the flame expands at a constant high speed from the onset of ignition. The flame is more nearly spherical than that for propane and the scale of the wrinkles is larger. Vilchis and Heywood also observed that the thickness of the turbulent burning zone in hydrogen was substantially thinner than that in propane. All of these observations are in qualitative agreement with the pre-

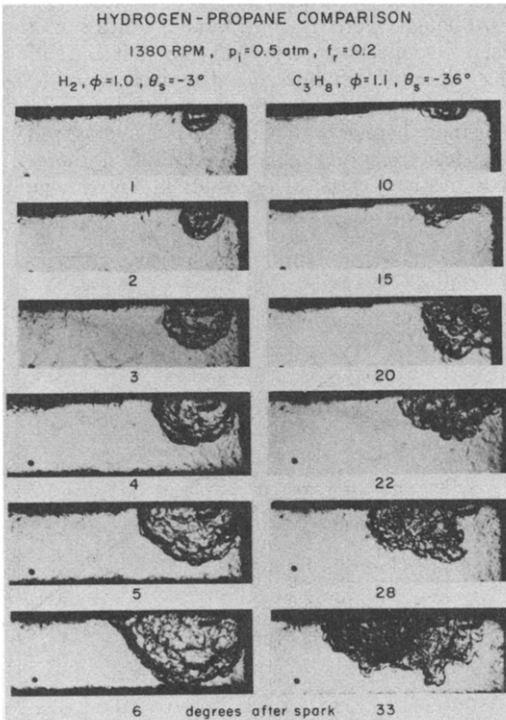


FIG. 16. Schlieren photographs made in M.I.T.'s square piston engine comparing the flame in hydrogen/air and propane/air mixtures at various crank-angles after spark.

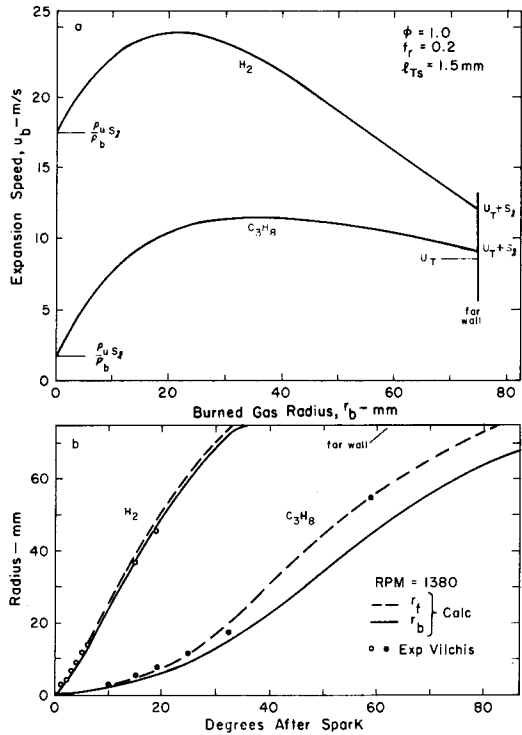


FIG. 17. (a) Calculated expansion speeds  $u_b$  for hydrogen/air and propane/air mixtures as a function of burned gas radius  $r_b$ . (b) Comparison of experimentally measured (points) and calculated (dashed curve) flame radii  $r_f$  for hydrogen/air and propane/air mixtures as a function of crank angle. Also shown (solid curve) is the burned gas radius  $r_b$ .

dictions of the burning equations 4.1 and 4.4.

A quantitative comparison of these measurements and the predictions of Eq. 4.1 is shown in Fig. 17. The calculated burned gas expansion speeds  $u_b$  for hydrogen and propane are shown as a function of burned gas radius in Fig. 17a. The parameters  $u_T$  and  $\ell_T$  were chosen to fit the propane data and are consistent with values shown in Figs 14 and 15. The laminar burning speeds for propane were obtained from Ref. 35. Those for hydrogen were obtained from recent measurements by Brian Milton made in M.I.T.'s spherical combustion bomb.

It can be seen that the initial expansion speed in hydrogen is roughly 10 times that in propane and that there is relatively little increase in this speed as the burning proceeds. This is in marked contrast to the expansion speed in propane which undergoes a large initial increase due to the large difference in the ratio  $u_T/s_\ell$  for these two gases. For propane,  $u_T/s_\ell \sim 10$  while for hydrogen,  $u_T/s_\ell \sim 1.0$ .

The results of integrating the curves in Fig. 17a are given in Fig. 17b. Both the burned gas radius  $r_b$  and flame radius  $r_f$  are shown as a function of crank angle after spark. Also shown are the experimental values of  $r_f$  obtained from the photographs in Fig. 16. As previously mentioned, the parameters  $u_T$  and  $\ell_T$  were chosen to fit the propane data. There were no free parameters involved in calculating the hydrogen curves. It can be seen that the agreement between the predictions and measurements is excellent and almost certainly in part fortuitous. It can also be seen that the difference  $(r_f - r_b)$  is very much smaller for hydrogen than propane. This is a simple consequence of the fact that for a quasi-steady premixed turbulent flame  $(r_f - r_b) \cong u_T \tau_b = u_T \ell_T / s_\ell$ .

### 5. Summary and Conclusions

Recent experimental investigations of turbulent flame structure and speed in spark-ignition engines have been analyzed. Optical observations made using schlieren and laser scattering techniques strongly suggest that the initial phase of combustion in such engines involves a relatively smooth spherical laminar flame. As the flame grows the flame front becomes increasingly distorted by the turbulent flow field through which it is propagating and develops a highly wrinkled and probably multiply connected structure. During this process the mean expansion speed increases rapidly from a value of order 1 m/s characteristic of a spherical laminar flame in the charge to a quasi-steady value of order 10 m/s characteristic of the turbulence intensity in the unburned gas. The thickness of the wrinkled zone is proportional to the ratio  $u_T/s_\ell$  of the turbulence intensity to the laminar burning speed and the lateral scale of the wrinkles is inversely proportional to this same ratio. For normal hydrocarbons such as propane and isoctane, the thickness of the wrinkled zone is of order 10 mm and the lateral scale of the wrinkles is of order 1 mm. There is no evidence of thick turbulent flames with a monotonic density gradient under any of the conditions studied to date.

Simultaneous pressure measurements and high speed motion pictures of the visible flame show that, for normal hydrocarbons, more than 20% of the gas entrained in the flame is unburned during the rapid quasi-steady burning phase of combustion. They also suggest that the final phase of combustion can be approximated by an exponentially decreasing burning rate with a time constant of order 1 ms.

Detailed analysis of this data has led to the development of two closely related sets of empirical burning equations 4.1 and 4.4. The first set suggests an eddy entrainment and laminar burn-out

model and the second, a laminar flame stretching and wrinkling model. Each set of burning equations contains four parameters: the laminar burning speed of the charge  $s_\ell$ , a characteristic speed  $u_T$ , a characteristic length  $\ell_T$  and a vector  $r_c$  giving the position of the apparent flame center. Measurements of  $s_\ell$  under engine-like conditions can be made in constant volume combustion bombs and values for a number of common fuels are already available. Values for  $u_T$  and  $\ell_T$  can be obtained from engine experiments and preliminary correlations for relating these parameters to engine geometry and operating variables are given in Figs 14 and 15. The data suggest that  $u_T$  increases and  $\ell_T$  decreases during compression of the unburned gas. The nominal value of  $r_c$  is determined by the spark plug position but convection of the flame kernel at early times can produce significant displacement.

For a given engine cycle, the parameters in either set of burning equations can be adjusted to fit the observed pressure curves within the accuracy of the measurements. Cycle-to-cycle fluctuations in pressure can be caused by variations in any of the parameters  $s_\ell$ ,  $u_T$ ,  $\ell_T$  and  $r_c$ . Variations in  $s_\ell$  are due primarily to incomplete mixing of the fresh charge with burned residual gas in the cylinder but can also be caused by variations in the stoichiometry of the fresh charge. Variations in  $u_T$  and  $\ell_T$  are presumably associated with the statistical character of turbulence. Variations in  $r_c$  are caused by random convection of the flame kernel in the flow field near the spark plug. In this connection it may be noted that a correlation of  $r_c$  with pressure has been observed in the laser-doppler measurements of Cole and Swords.<sup>[38]</sup>

Although, in the opinion of the author, the experimental data presented provides convincing evidence for the wrinkled structure of turbulent flames in spark-ignition engines and the empirical burning equations proposed provide a relatively simple and accurate method for predicting the burning rate in such engines, the range of engine geometries and operating variables investigated to date is relatively small and needs to be considerably extended. Systematic investigations over a wider range of engine speeds, spark angles, valve lifts and compression ratios are needed to check the tentative correlations for  $u_T$  and  $\ell_T$  given by Eqs 4.10 and 4.11. The origin of the dispersions in all four parameters  $s_\ell$ ,  $u_T$ ,  $\ell_T$  and  $r_c$  needs to be more closely examined and correlations for relating the magnitude of their dispersions to engine geometry and operating variables developed. The applicability of the burning equations to engines with significant swirl and squish needs to be studied. Finally, the physical basis of the empirical burning equations and their relation to more fundamental theories of turbulent combustion need to be investigated.

## Nomenclature

A	area
$A_c$	area of "best fit" circle
$A_{IV}$	maximum open area of inlet valve
$b$	bore
CR	compression ratio
$D_{IV}$	inlet valve diameter
$f_r$	residual burned gas fraction
$h$	clearance height
$\ell_T$	characteristic length
$L_c$	arc length of "best fit" circle
$L_{IV}$	maximum inlet valve lift
$m$	mass
N	engine speed (revolutions/time)
$p$	pressure
$r$	radius
$r_c$	radius of center of "best fit" circle
$s$	entrainment speed
S	stroke
$t$	time
T	temperature
$u$	expansion speed
$u_T$	characteristic speed
V	volume
$\omega$	angular speed
$x$	mass fraction
$y$	volume fraction
$\epsilon_c$	volumetric efficiency
$\theta$	crank angle
$\eta$	parametric area
$\mu$	parametric mass
$\rho$	density
$\tau_b$	characteristic burning time
$\tau_T$	characteristic flow time
$\chi_c$	azimuth of center of "best fit" circle

## Subscripts

$b$	burned gas
$f$	observed flame
F	far wall
$i$	inlet condition
$m$	motored
$\ell$	laminar
$p$	piston
$s$	spark condition
$u$	unburned gas
$v$	combustion chamber

## Acknowledgment

The author would like to thank Dr. Alun Thomas for numerous delightful and illuminating discussions about the concept of flame stretching and its application to turbulent combustion in spark-ignition engines. These discussions, which took place during the author's 1979-80 sabbatical year at Churchill College in Cambridge, England, pro-

vided the motivation for developing burning equations of the form 4.4. He would also like to thank Sir William Hawthorne for inviting him to Churchill College, Dr. Brian Milton for his timely measurements of the laminar burning speed of hydro- gen at high pressure and Professor J. B. Heywood, Dr. J. R. Smith and Dr. P. O. Witze for supplying additional information about their experiments and the photographs reproduced in this paper.

## REFERENCES

1. "Combustion Modeling in Reciprocating Engines" (J. N. Mattavi and C. A. Amann, eds), Plenum Press, 1980.
2. ANDREWS, G. E., BRADLEY, D. AND LWAKA-BAMBA, S. B., *Combustion and Flame* 24, 285 (1975).
3. TABACZYNSKI, R. J., *Prog. Energy Combust. Sci.* 2, 143 (1976).
4. TABACZYNSKI, R. J., TRINKER, F. H. AND SHANON, B. A. S., *Combustion and Flame* 39, 111 (1980).
5. BRAY, K. N. C., "Turbulent Reacting Flows" (P. A. Libby and F. A. Williams, eds), Springer-Verlag, 1980.
6. LIBBY, P. A. AND BRAY, K. N. C., *AIAA J.* 19, 205 (1981).
7. ASHURST, W. T., Paper WSS/CI 81-23 presented at the Spring Meeting of the Western States Section of the Combustion Institute, April 1981.
8. LIBBY, P. A. AND WILLIAMS, F. A., *Combustion and Flame* 44, 287 (1982).
9. MOREL, T. AND MANSOUR, N. N., SAE paper 820040 presented at the International Congress and Exposition, February 1982.
10. BLIZARD, N. C. AND KECK, J. C., SAE paper 740191 presented at the Automotive Engineering Congress, February 1974.
11. LANCASTER, D. R., KRIEGER, R. B., SORENSON, S. C. AND HULL, W. L., Paper No. 760160 SAE Trans. 85, 689 (1976).
12. MATTAVI, J. N., GROFF, E. G., LIENISCH, J. N., MATEKUNAS, F. A. AND NOYES, p. 537 Ref. 1.
13. GROFF, E. G. AND MATEKUNAS, F. A., Paper No. 800133, SAE Trans 89, 740 (1980).
14. RASHIDI, M., The Institution of Mechanical Engineers, *Proceedings* 194, 231 (1980). See also *Combustion and Flame* 42, 111 (1981).
15. NAMAZIAN, M., HANSEN, S., LYFORD-PIKE, E., SANCHEZ-BARSE, J., HEYWOOD, J. AND RIFE, J., SAE paper 800044 presented at the International Congress and Exposition, February 1980.
16. WITZE, P. O., SAE paper 820044 presented at the International Congress and Exposition, February 1982.
17. SMITH, J. R., SAE paper 820043 presented at the International Congress and Exposition, February 1982.

18. RASSWEILER, G. M. AND WITHROW, L., SAE Trans. 42, 5 (1938).
19. MORI, T. AND YAMAZAKI, K., JSME 13, 600 (1970).
20. OHGASHI, S. AND HAMAMOTO, Y., JSME 13, 1232 (1970).
21. INUMA, K., JARI TM 2, 79 (1971).
22. MATSUOKA, S., YAMAGUCHI, T. AND UMIMURA, Y., Paper 710586 SAE Trans (1971).
23. IINUMA, K. AND IBA, Y., JARI TM 10, 59 (1972); *ibid* 15, 44 (1973).
24. ARRIZONI, V., CALVI, F., CORNETTI, G.M. AND POZZI, U., SAE Paper 730088 presented at the International Automotive Engineering Congress, January 1973.
25. NAKANISHI, K., HIRANO, T. AND INOUE, T., SAE paper 750054 presented at the International Congress and Exposition, February 1975.
26. NAKAMURA, H., OKINOUE, T. HORI, K., KIYOTA, Y., NAKAGAMI, T., OKISHINO, K. AND TSUKAMOTO, Y., Paper 780007 SAE Trans 87, 16 (1978).
27. CHAIBONGSAI, S., KADOTA, T. AND HENEIN, N. A., Paper No. 800860 SAE Trans 89, 2617 (1980).
28. FAGELSON, J. J., MCCLEAN, W. J. AND DEBOER, P.C.T., Comb. Sci. and Tech. 18, 47 (1978).
29. GIRGIS, N. S. AND TIDMARSH, D. H., I. Mech. E. Conf. on "Fuel Econ. and Emiss. of Lean Burn Engines," June 1979, Proceedings p. 185.
30. HEIKAL, M. R., BENSON, R. S. AND ANNAND, W. J. D., I. Mech. E. Conf. on "Fuel Econ. and Emiss. in Lean Burn Engines," June 1979, Proceedings p. 195.
31. BOWDITCH, F. W., Paper No. 150B, SAE Trans. 69, 17 (1960).
32. BERETTA, G. P., RASHIDI, M. AND KECK, J. C., Paper WSS/CI 80-20 presented at the Spring Meeting of the Western States Section of the Combustion Institute, April 1980.
33. BERETTA, G. P., RASHIDI, M. AND KECK, J. C., Sloan Laboratory Report, No. 110, M.I.T., 1982.
34. LAVOIE, G. A., HEYWOOD, J. B. AND KECK, J. C., Combust. Sci. and Technology 1, 313 (1970).
35. METCHALCHI, M. AND KECK, J. C., Sloan Laboratory Report No. 104, M.I.T., 1982.
36. THOMAS, A., "A Theoretical Study of the Influence of Operating and Design Variables on the Duration of Combustion in the Spark Ignition Engine," University of Cambridge Technical Report, CUED/AThermo/TR12, 1979.
37. VILCHIS, F. R., "Comparative Study of Hydrogen and Propane Combustion in a Transparent Quartz-Walled Spark-Ignition Engine," M.S. Thesis, Mech. Eng., Mass. Inst. of Tech., February 1982.
38. COLE, J.B. AND SWORDS, M.D., SAE paper 800043 presented at the International Congress and Exposition, February 1980.

## COMMENTS

*Prof. N. Chigier, Carnegie-Mellon University, Pittsburgh, PA.* Do you believe that the flame front photographs can be used to determine dimensions of large scale structures in the flow? Also can you suggest a physical relationship between a series of photographs of the flame front and local measurements of turbulence intensity of laser anemometer?

*Author's Reply.* To answer your first question I would have to know how you propose to separate large and small scale structures along a flame front. Photographs such as those in Figs 3-5 tend to show a more or less continuous distribution of scales. One could of course expand the structure in terms of cylindrical harmonics and this might be a useful thing to do. In fact the fitting of a circle to the flame front is just the first step in such an expansion.

In answer to your second question I believe that the characteristic speed  $u_f$ , deduced from the quasi-steady propagation speed of the flame front will

turn out to be proportional to the turbulence intensity measured by a laser anemometer. Moreover preliminary comparisons which have been made suggest a correlation coefficient close to unity.

*Prof. R. W. Bilger, University of Sydney, Australia.* I was very pleased to see that you think so much of Ray Smith's work at Sandia, as I have followed it closely and have been very excited by it. One conclusion that he draws from his measurements is that the flame is instantaneously thicker than that for a laminar flame, particularly at higher engine speeds. This is after allowing for the effects of flame front angle. Why do you reject these findings? Would the bases for your empirical correlations be invalidated if in fact the flame is thickened by the small scale turbulence (as in Dam Kohler's second mechanism) and presumably the local flame front speed increased?

*Author's Reply.* The conclusion that the thickness of the reaction front separating unburned and burned gases increase with engine speed depends critically on the form of the distribution function used to correct the data for the effect of tilted fronts. In making this correction Smith assumed a Gaussian distribution with respect to the tilt angle. I do not believe this is a good assumption. It seems to me that a much better assumption would be a Gaussian distribution with respect to the solid angle available for the unit vectors normal to the front. In this case the most probable tilt angle is not zero as Smith assumed but a finite angle whose magnitude increases as the engine speed and hence the degree of wrinkling of the front increases. This could lead to a large increase in the apparent thickness of the observed fronts. Whether an additional contribution due to an increase in the intrinsic thickness of front would be required to explain the observations is unclear, however.

The only place where the thickness of the reaction front enters the present analysis is in the thermodynamic model used to calculate the burned gas mass fraction from the observed pressure. Here it is explicitly assumed that the volume of the reaction zone is small compared to the combustion chamber volume. For this to be seriously in error, fronts many times thicker than those calculated by Smith would be required. In any case only the value of the characteristic length  $\ell_T$  would be affected and the structure of the empirical burning equations would not be changed.

●

*Dr. Omer L. Gulder, Division of Mechanical Council of Canada.* I have a question related to a

simple detail in your correlation, since I understand your flame velocity is a function of a characteristic speed  $u_T$  and laminar burning velocity. Since the effect of the  $u_T$  seems to be much larger than that of laminar burning velocity and  $u_T$  is a function of hydrodynamic properties and velocity, I wonder how your correlation can handle the effect of mixture strength on flame speed. Is it necessary to add a term to your correlation in order to account for different equivalence ratios or does the correlation handle it by its present form?

*Author's Reply.* The characteristic speed  $u_T$  is primarily important for determining the quasi-steady speed of the fully developed wrinkled flame. At early times before significant wrinkling of the front has occurred, the flame propagates at expansion speed of a laminar flame which is, of course, a function of equivalence ratio. The burning equations were constructed to reproduce this behavior and no additional dependence on equivalence ratio beyond that contained in the laminar burning speed is required to fit the available data. In this connection it may be noted that unless the equivalence ratio is very close to an ignition limit, the fuel type and the residual burned gas fraction have a larger effect on the laminar burning speed than the equivalence ratio. The effect of fuel type is most dramatically illustrated in Fig. 17 where burning rates in hydrogen/air and propane/air mixtures are compared. The effect of residual burned gas fraction can be seen in Fig. 8 where burning rates for the first and subsequent cycles are compared. In each case it is the induction delay which is most strongly affected by the change in the laminar burning speed. The quasi-steady burning rates are relatively insensitive to the laminar burning speed.